



## Estimation of Air Temperatures for the Urban Agglomeration of Athens with the Use of Satellite Data

Agathangelidis I\*, Cartalis C<sup>1</sup> and Santamouris M<sup>1</sup>

### Abstract

Changing air temperature trends within urban regions deserve careful monitoring as they may reflect modifications in the thermal environment, including the development of an urban heat island. Air temperature fields need to be dense in order the state of the thermal environment to be adequately assessed; yet in most cases, the networks of ground measuring stations are sparse. This paper attempts to define the relationship between downscaled land surface temperature (LST) at resolution 1 km as deduced from MSG-SEVIRI satellite images, and air temperature ( $T_{air}$ ) in the urban agglomeration of Athens, for varying land cover types. Polynomial regression and artificial neural networks are used to estimate  $T_{air}$  from LST at a particular time, whereas the LST values for several hours before are also used. In this way, the “memory” of the surface materials is taken into consideration, practically reflecting the thermal inertia associated with land cover. For urban stations, an average  $R^2$  of 0.85 and an RMSE of 1.0-1.2°C was achieved for the majority of the examined time period, an indication of both the capacity of the methodology to define  $T_{air}$  fields in the area under consideration as well as of the fact that LST is the controlling parameter for  $T_{air}$ . The parametric relations as extracted from the above methodology are in principle applicable for a specific station, as they depend on the land cover and the associated land surface characteristics. They may be also used for stations in areas with similar land cover and in the same climatic zone.

### Keywords

Remote sensing; Urban climate; Land surface temperature; Air temperature

### Introduction

The thermal environment is a significant part of the urban environment; it is a reflection of the surface and atmosphere energy balance as well as of the energy fluxes between the surface and the atmosphere close to the surface [1]. Elevated temperatures in urban areas enhance photochemical pollution and increase the energy needs for cooling [2,3]. In addition, a well-documented phenomenon in cities is the urban heat island (UHI), which refers to higher LST and air temperatures ( $T_{air}$ ) in the city as compared to the rural surroundings [1]. For Athens a mean intensity of 5.6°C has been reported for the

surface urban heat island (SUHI) during summer months using satellite remote sensing [4], while a summer daytime UHI amplitude growing rate of 0.8°C per decade has also been found [5]. The much higher sensible heat flux values compared to latent heat flux expected in Athens have been validated in energy budget experiments [6]. LST has been found to be up to 5°C lower than  $T_{air}$  during summer nights and up to 15°C higher during the rest of the day [7]. Weather prediction models have recently also been used in order to simulate the thermal environment of Athens [8,9]. Studies attempting to assess the effect of local scale and mesoscale phenomena on the UHI of the area have reported that both sea breeze and anticyclonic conditions tend to reduce the UHI intensity [10].

The ambient temperature in urban areas presents a strong spatial variability because of the variable thermal balance of the various urban zones [11]. Several studies have shown that the ambient temperature may fluctuate several degrees even in small zones of several hundred meters [12]. Knowledge of the exact spatial distribution of the ambient temperature is of crucial importance for energy, comfort and environmental reasons. Higher urban temperatures have a serious impact on the energy consumption of buildings spent for cooling purposes and may increase up to 100% the corresponding energy demand [13]. Proper design of the auxiliary heating and cooling systems requires a full knowledge of the local temperature conditions in order to avoid over or under sizing of the auxiliary energy components. In parallel, design and implementation of adequate mitigation systems in open spaces and buildings requires a complete knowledge of the local thermal conditions in order to counterbalance properly the impact of urban heat island [14]. Furthermore, it is well known that higher local temperatures affect strongly local comfort conditions while may cause increased pollution levels and in particular higher ozone concentrations [15,16]. Thus, knowledge of the local thermal conditions is essential for the planning and implementation of the urban resilience plans. Finally, the study of  $T_{air}$  in the urban environment is highly important in view of the observed worldwide urbanization trends. Correlation analysis between LST, albedo, emissivity and land cover indices has been found to provide important insights regarding urban UHI [17], while the use of gridded  $T_{air}$  values could be a further aid.

$T_{air}$  is provided by ground measuring stations; yet in many urban areas the network of ground measuring stations is sparse, a fact which limits a full depiction of the  $T_{air}$  field within the urban boundaries. Satellite remote sensing on the other hand allows the estimation of LST at spatial resolutions ranging from 60 m × 60 m to 1 km × 1 km, with the respective temporal resolutions ranging from 16 days to few hours. To this end, it is important to examine the relationship between LST and  $T_{air}$  in an urban area, taken that a statistically significant relationship may in practice allow the construction of  $T_{air}$  fields at higher spatial resolution compared to the respective one of the network of ground stations.

Drawbacks may well arise, mostly with respect to modifications in land cover, a fact which may impose constraints to the applicability of the defined relationship as the type of land cover influences latent and sensible heat, the emission of thermal radiation from the ground and finally the capacity of the ground surface to retain heat once acquired. To this end, relationships of this kind need also to indirectly integrate

\*Corresponding author: Agathangelidis I, Department of Environmental Physics, University of Athens, Panepistimiopolis, Build PHYS-V, Athens 15 784, Greece, Tel: +30 2107276774; E- mail: ilias\_aga@yahoo.gr, msantam@phys.uoa.gr, ckartali@phys.uoa.gr

Received: December 23, 2015 Accepted: March 14, 2016 Published: March 21, 2016

the “memory” of the thermal state of the surface, i.e. the temperature values of LST at times prior to the estimation time. Such integration may reflect the type of land cover and the thermal capacity of the ground.

In the last decades several studies have attempted to estimate  $T_{air}$  using satellite remote sensing data. Chen et al. [18] used simple linear regression models between LST from GOESS satellites and air temperature at 1.5 m height, over a four winter period (1978-1981) in Florida, USA. They reported a mean correlation coefficient of 0.87 and an average sample standard deviation from regression of 1.57°C. Green et al. [19] used the normalized difference vegetation index (NDVI) together with LST. The data used were from the AVHRR sensor of NOAA satellites, between 1988 and 1992, over Africa and Europe and the root mean square error (RMSE) found ranged from 1.83°C to 3.18°C. Many other studies have also used vegetation data and several of them have followed the Temperature Vegetation Index (TVX) method [20,21], which assumes that NDVI presents a linear correlation with LST. Moreover, remote sensing techniques have been used in order to estimate air temperatures in a UHI. For example Pichierrri et al. [22] made use of MODIS brightness temperature, in order to monitor canopy layer temperatures for the years 2007-2010. The study domain was the city of Milan, Italy; an RMSE from 1.2°C to 1.8°C was estimated. Bechtel et al. [23] used multi temporal MSG-SEVIRI LST data over Hamburg, Germany and reached an RMSE of 1.5-1.8°C with explained variances of 97-98%. Good [24] estimated daily air temperature minima and maxima over Europe for 2012-2013 with the use of such predictor variables as LST, fraction of vegetation, latitude, elevation and urban fraction. The latter were regressed against air temperature resulting in RMSE of about 2.5°C. Sun et al. [25] used a different approach than most studies, as they utilized thermodynamic parameters along with MODIS data for the North China Plain. They succeeded an accuracy of better than 3°C for 80% of the derived air temperatures.

### Area of Study and Data Sources

The study region of this paper is the urban agglomeration of Athens, Greece (37°58'N, 23°43'E), an area of about 412 km<sup>2</sup> with population of four million inhabitants. Athens is located in the southeastern end of the Greek mainland, in the Attica basin (Figure 1). The city is bounded by mountains to the north, northeast and east directions and by the Saronic Gulf to the southwest. Athens experiences a typical Mediterranean climate with mild, relatively wet winters and hot, dry summers. The average temperature during summer is about 28°C, while the daily maximum temperature in July and August exceeds 33°C.

For the purposes of the study, satellite (in total 8092 LST images for the summers of 2014 and 2015) and ground data were used for a selected period. Satellite data originate from the geostationary Spinning Enhanced Visible Infra-Red Imager (SEVIRI) sensor onboard the Meteosat Second Generation (MSG) satellites. SEVIRI has twelve spectral channels covering visible and infrared wavelengths with a high temporal resolution of 15 minutes and a spatial resolution of 3-5 km. An operational LST product at an enhanced spatial resolution (1 km) was used, provided by the Institute for Astronomy, Astrophysics, Space Applications and Remote Sensing (IAASARS) of the National Observatory of Athens (NOA). The methodology of the NOA/IAASARS system is described in Keramitsoglou et al. [26,27]. In brief:

(a) Real time acquisition and preprocessing of raw MSG-SEVIRI data results in radiance images at a spatial resolution of 3-5 km

depending on the distance from the sub-satellite nadir viewpoint.

(b) Cloud-free data are then used for estimating LST by employing the Operational version of the Automated Atmospheric Absorption Atlas (4A/OP) line-by-line radiative transfer model and a support vector regression (SVR) machine, and

(c) downscaling of the LST images is succeeded by employing an algorithm that upscales ancillary static and dynamic datasets (e.g. land cover, elevation, slope, vegetation indices, etc.) with fine spatial resolution (1 km) to the MSG-SEVIRI geometry and then uses a regression model to fine scale ancillary datasets.

The improvement of the initial coarse spatial resolution of MSG-SEVIRI imagery is considered necessary due to the need for detailed spatial information.

In terms of the ground data, air temperature observations from 7 weather stations (Figure 2), part of NOA network stations, were acquired. The selection of the stations was made taking into account their location so as to include areas of varying land cover. In particular, three stations are located in the most densely populated region of the city, two stations in the suburban area and two stations in peri-urban areas. Further details of the stations can be seen in Table 1. The temperature sensors used, were part of the Davis Vantage Pro2 weather stations installed at the selected case study locations.

Finally, the Urban Atlas land cover data from the European Environment Agency were also used [28]. The initial 20 land cover classes of the database were merged into the 3 classes of study interest (urban, suburban, peri-urban) (Figure 3). Land cover data were upscaled to 1 km and projected to the same coordinate system (UTM, ED50) with MSG-SEVIRI images in order to be used in conjunction with the latter.

### Methodology and Results

The relationship between  $T_{air}$  and LST is rather complex, determined mostly by the surface energy budget. The vast number of parameters involved (e.g. wind speed, surface roughness, atmospheric stability) as well as the complicated urban geometry makes an analytical approach to the problem very demanding. A simplification can be achieved

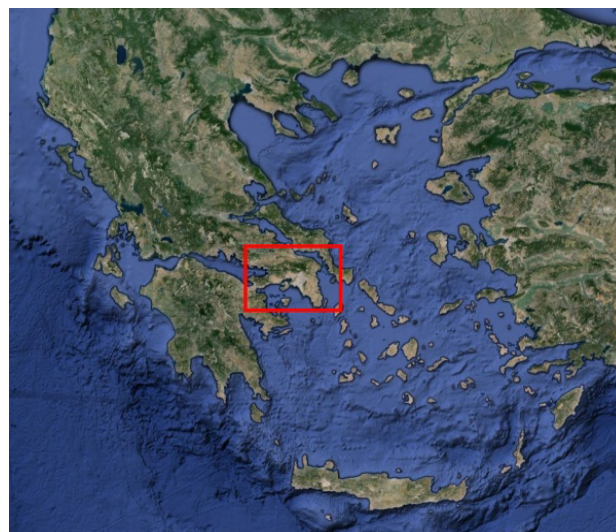


Figure 1: Study area.

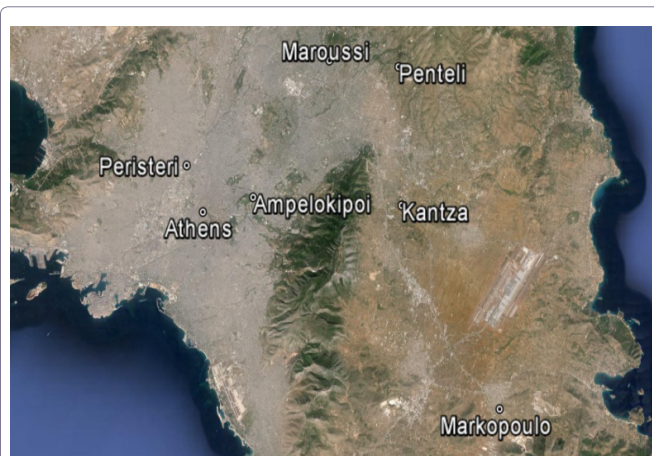


Figure 2: Locations of the 7 used weather stations.

Table 1: Characteristics of weather stations.

Location	Latitude	Longitude	Elevation (m)	Type
Ampelokipoi	37° 59' 06" N	23° 45' 14" E	136	urban
Athens	37° 58' 42" N	23° 42' 56" E	50	urban
Kantza	37° 58' 45" N	23° 51' 56" E	221	peri-urban
Markopoulo	37° 52' 37" N	23° 56' 13" E	104	peri-urban
Maroussi	38° 03' 06" N	23° 48' 47" E	235	suburban
Penteli	37° 02' 50" N	23° 51' 53" E	495	suburban
Peristeri	37° 00' 06" N	23° 42' 14" E	55	urban

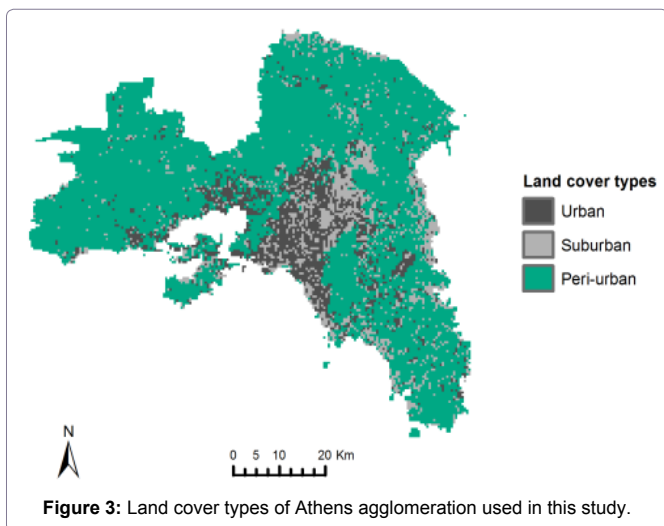


Figure 3: Land cover types of Athens agglomeration used in this study.

considering statistically based methods and artificial neural networks. In this study, the estimation of  $T_{air}$  from LST on the basis of the multitemporal approach of [23] was attempted with the use of:

### Polynomial regression

In particular and taking advantage of the high temporal resolution of MSG-SEVIRI data, a multi-temporal approach was followed leading to sets of parametric relations. According to this method,  $T_{air}$  at a particular hour is calculated using the LST value of the same hour, as well as the LSTs of previous hours (acting as predictors). The physical basis of this approach lies in the fact that part of the heat stored in urban structures will be released a few hours later, warming the air above.

### Artificial neural networks

A feed forward network was developed using as input and output layer entries LST and  $T_{air}$  respectively, with a hidden layer of 10 neurons. The network was trained by adjusting the weights in the hidden layer so as the output values errors to be as small as possible. The architecture of the two-layer neural network is described as follows: The LST values were used as the vector input of the network, where each neuron of the hidden neurons layer is connected with the individual vector elements, as the latter are multiplied with the adjustable neuron weights. The weighted values are then summed with the neuron bias to form a net input. This value is then the argument of the sigmoid transfer function selected for the hidden layer. The output of this layer subsequently serves as the input of the following layer where the previous procedure is repeated, this time using a linear transfer function. The final output of the neural network is programmed to be equal to the air temperature data of the weather station selected in each particular case. The training of the neural networks was accomplished using the Levenberg-Marquardt algorithm as it can provide fast convergence. The multitemporal approach described in the previous paragraph, was also employed.

At a first stage, the missing, due to cloud cover, LST images were detected and the gaps were filled using blank values in order to construct a continuous time series. Following and on the basis of the geographical coordinates of the weather stations, the corresponding pixels from the stack of images were extracted and the  $T_{air}$  time series were resampled and synchronized with the created LST series. Finally, the data were divided into a training dataset used for the derivation of parametric relationships between LST and  $T_{air}$  (01.06.2014 – 15.08.2014) and testing sets used for validation of these relations (16.08.2014 – 31.08.2014, 01.07.2015 – 31.08.2015).

In order to assess the accuracy of the models output, a number of different statistical measures were used such as the coefficient of determination ( $R^2$ ), the Root mean square error (RMSE) and the Mean absolute error (MAE).  $R^2$  gives the fraction of the total air temperature variance that can be explained by the predictors, RMSE is defined as the square root of the mean of squared differences between the air temperature values predicted from the model and those measured at the weather stations and MAE is the mean of the absolute differences between the two above mentioned temperatures. Mean error (ME) was also used, defined as the mean of the differences between the model and station temperatures. Finally and in order to use an error metric which is not dependent on the values scale, the normalized mean absolute error was calculated (NMAE). The normalization was performed dividing MAE with the mean value of the *in situ* air temperature observations. Following the same logic the normalized mean error (NME) in % was also calculated.

Using the training dataset, an examination of the influence of the order of regression to the quality of the fit between  $T_{air}$  and LST was made, while using a monotemporal approach. It was estimated that the use of 5<sup>th</sup> order compared to 1<sup>st</sup> order regression improved  $R^2$  by 0.04-0.05 for the majority of the stations (Figure 4), while RMSE and MAE errors were reduced by an average value of 0.2°C. In addition, by dividing the results into daytime and nighttime hours, it was deduced that the order of regression played an important role mostly in the nighttime data.

The different partitioning of energy into sensible and latent heat led to distinct relations depending on the station land cover type. For instance, a linear relationship of the form  $T_{air} = 0.43 \cdot LST + 15.96$

was derived for an urban station (Ampelokipoi), while for suburban (Penteli) and peri-urban (Kantza) stations the respective relations were  $T_{air} = 0.41 \cdot LST + 13.87$  and  $T_{air} = 0.52 \cdot LST + 12.59$ .

It was also found that the transfer of parametric relationships between stations with similar land cover (and subsequently land surface characteristics) resulted in slight error increases (0.05-0.2°C for urban stations).

Following, the multi-temporal approach was used, with the results being significantly better, as  $R^2$  improved by 0.15. The adjusted  $R^2$  was also calculated so as to ensure that the improvement was not artificial due to the increasing number of degrees of freedom and found almost equal to  $R^2$ . The error values when adding more independent variables were constantly decreasing. Detailed results for 2<sup>nd</sup> order regression can be seen in Table 2, where the following notation is followed: LST-0 corresponds to the monotemporal model, while, for example, LST-4 stands for a predictor set of the LST value simultaneous to  $T_{air}$  and for 1, 2, 3 and 4 hours before.

It should be mentioned that the ME error is approximately zero, as at this stage of the study the model uses the training dataset and thus has almost no bias.

Errors for all cases were about 0.4°C lower at night in comparison with day, due to the weak turbulent advection during those hours. Moreover, the performance of the multitemporal models was substantially better for the stations located in the most populated region of the city, especially for the hours after sunset.

NMAE errors ranged from 4.5% for Athens to 6.1% for Penteli for the monotemporal 2<sup>nd</sup> order model while for the LST-8 model the respective errors were 3.4% and 4.7%.

Table 3 shows the derived parametric relations for multiple linear regression using the LST-4 predictor set. The use of artificial neural networks gave slightly better results compared to regression models for all weather stations. The average results for all predictor sets for both regression and neural networks models are shown in Figure 5.

For validation purposes, the performance of the derived parametric relationships between LST and  $T_{air}$  was assessed using an independent data set of the same year (16.08.2014-31.08.2014). Results of the validation for this case were highly satisfactory reaching an MAE below 1°C for 6 of the 7 stations using the best performing algorithm. Similar findings as in the training phase were observed, i.e. improved model output values for nighttime data and for urban stations as well as smaller errors when using neural networks. ME ranged from about -0.3°C (underestimation) to 0.2°C (overestimation) depending on the model and the station.

Figure 6 shows that the modeled  $T_{air}$  (neural networks, predictor set: LST-8) for an urban weather station, follows very well the in situ measured temperature with no particular systematic bias. Detailed statistical metrics for the multitemporal LST-8, 2<sup>nd</sup> order regression model are presented in Table 4. As seen from ME and NME, all stations suffer a small overestimation in this predictor set, while the use of NMAE reinforces the previous findings, namely that the models have better accuracy for the urban stations compared to suburban and peri-urban ones.

A slight increase in the error (about 0.1-0.2°C) was observed once LST was estimated from the values of LST in the previous 4 hours and thereafter used for the estimation of  $T_{air}$ . Transferring the derived parametric relations from one station to another of similar land cover

types resulted in a small increase in error, for instance an average increase of 0.1°C was found between urban stations.

Validation results for July and August of 2015 were also satisfactory as the estimated MAE using the best performing model for these months was approximately 1.2°C for the urban stations and up to 2°C for the suburban ones. As seen in the distribution of residuals (predicted  $T_{air}$  minus observed  $T_{air}$ ), a slight overestimation was found (Figure 7). It should be mentioned however that larger errors may arise in the event of limited available data (for instance due to extended cloud cover) as well as of higher than average LSTs during the study period. It is also important to note that in 2015, the neural network models performed worse than the regression, a fact which may be attributed to over-fitting problems. A heat wave event which occurred during this study period (at 30<sup>th</sup> and 31<sup>st</sup> of July) was selected for the development of 1 km spatial resolution LST and  $T_{air}$  maps. The previously derived parametric relations (LST-3 regression model) for the most representative station of each land type (urban: Ampelokipoi, suburban: Maroussi, peri-urban: Kantza) were applied in every image pixel. The selection of the suitable relation was made detecting each pixel land cover type using the Urban Atlas data. As seen in Figure 8, both surface and (simulated) air temperature spatial patterns reveal that during daytime (12.00 UTC, 15.00 local time) the highest temperatures are found outside the urban center. In particular, two hot spots are located western of Athens (Megara, Elefsina-Aspropyrgos) and one eastern of the city (Mesogeia). Megara and Mesogeia are mostly agricultural lands composed of low vegetation while Elefsina-Aspropyrgos is an industrial zone. These areas warm up faster than the urban center where the high thermal capacity of building materials results in a negative heat island (Cool Island) at 12.00 UTC. The air temperature map provides more information regarding points of high thermal stress, as the parametric relations between LST and  $T_{air}$  have potentially incorporated additional heating effects often correlated with land cover, for example anthropogenic heat sources due to road traffic or cooling units. The lower temperatures at the coastline could

Table 2: Results of 2<sup>nd</sup> order regression multitemporal models, (training set: 01.06.14-15.08.14).

Stations	Predictor sets											
	LST - 0			LST - 2			LST - 4			LST - 8		
	$R^2$	RMSE (°C)	MAE (°C)	$R^2$	RMSE (°C)	MAE (°C)	$R^2$	RMSE (°C)	MAE (°C)	$R^2$	RMSE (°C)	MAE (°C)
Ampelokipoi	0.77	1.59	1.24	0.81	1.41	1.10	0.83	1.36	1.04	0.86	1.21	0.90
Athens	0.78	1.55	1.19	0.81	1.44	1.08	0.82	1.40	1.05	0.85	1.27	0.93
Kantza	0.82	1.86	1.43	0.84	1.78	1.35	0.85	1.74	1.33	0.87	1.62	1.23
Markopoulo	0.81	1.66	1.30	0.84	1.51	1.16	0.85	1.44	1.10	0.88	1.31	0.98
Maroussi	0.77	1.69	1.31	0.83	1.44	1.12	0.85	1.37	1.05	0.88	1.21	0.89
Penteli	0.72	1.88	1.49	0.76	1.74	1.36	0.78	1.67	1.29	0.81	1.51	1.14
Peristeri	0.76	1.59	1.23	0.79	1.49	1.13	0.80	1.46	1.10	0.82	1.37	1.03

Table 3: Multiple regression coefficients of the parametric relationship  $T_{air} = \alpha + \alpha_0 \cdot LST_0 + \alpha_1 \cdot LST_1 + \alpha_2 \cdot LST_2 + \alpha_3 \cdot LST_3 + \alpha_4 \cdot LST_4$ , LST subscript corresponds to hours before  $T_{air}$  measurement.

Stations	Coefficients					
	$\alpha$	$\alpha_0$	$\alpha_1$	$\alpha_2$	$\alpha_3$	$\alpha_4$
Ampelokipoi (urban)	14.04	0.34	0.05	0.00	-0.03	0.16
Penteli (suburban)	12.55	0.33	0.06	0.00	-0.02	0.12
Kantza (peri-urban)	10.77	0.49	0.18	-0.15	-0.20	0.28

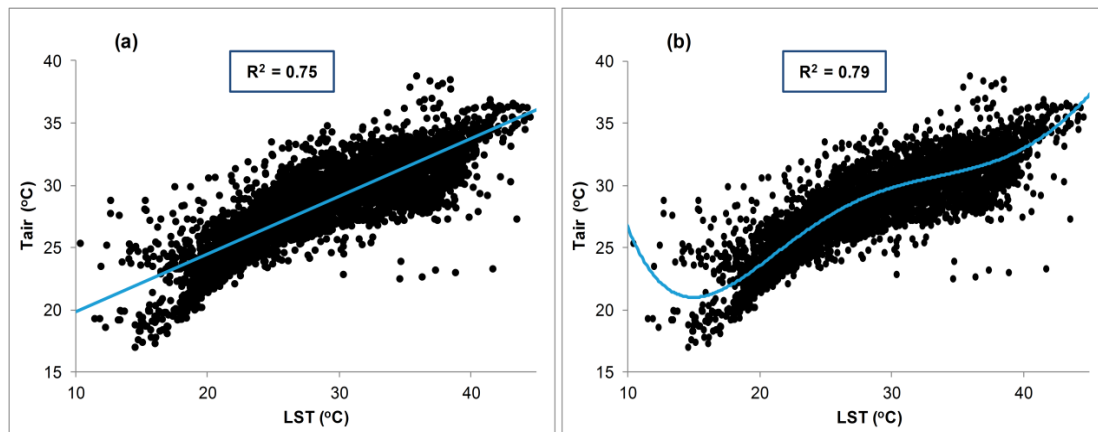


Figure 4: Scatter plot, Athens station (01.06.14-15.08.14): a) Linear regression, b) 5<sup>th</sup> order regression.

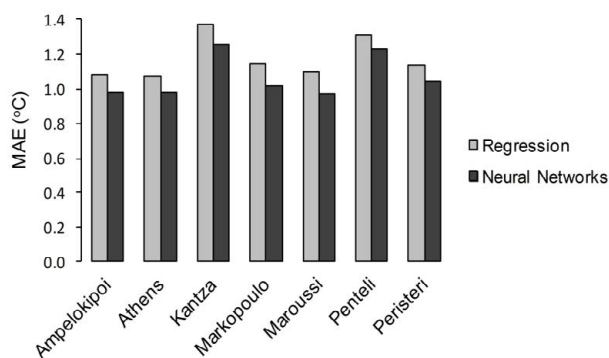


Figure 5: Mean performance of all used predictor sets (training phase), MAE (°C).

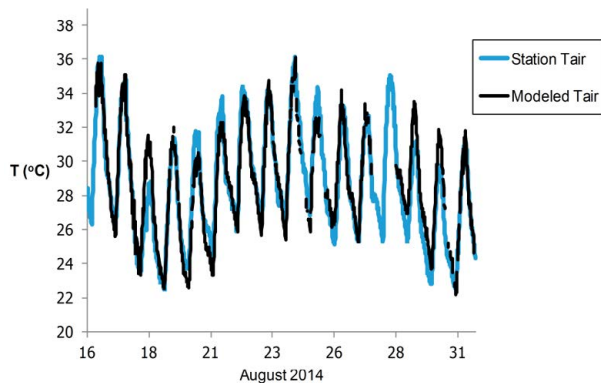


Figure 6: *In situ* and modeled air temperature for Ampelokipoi station, 16.08.14-31.08.14 (neural networks, LST-8 predictor set).

be ascribed to sea breeze. At night (00.00 UTC, 03.00 local time) the situation is reversed and the city center exhibits the highest LST and (simulated) air temperatures (Figure 9). In particular, the residential zones at the center and the south part of the city are subjected to a very strong heat island effect which can be seen more distinctly at the air temperature spatial map, as the heat being absorbed and stored within the urban fabric during daytime is released warming up the canopy layer air.

## Conclusions

In this study, a methodology for estimating urban  $T_{air}$  from LST, the latter extracted from satellite measurements, is applied. Polynomial regression and neural network models were developed using downscaled 1 km LST SEVIRI data and in situ air temperature measurements from ground-based stations in the urban agglomeration of Athens. Results highlighted that adopting a multi-temporal approach, i.e. estimating  $T_{air}$  taking into account the same time LST as well as the LSTs of previous hours, improved substantially the model output. For urban stations an average  $R^2$  of 0.85 and an RMSE of 1.0-1.2°C was achieved for the majority of the examined time period, using the best performing algorithms. The accuracy of the models was found to be higher for stations at the most densely populated area of the city, a fact which can be explained by the high thermal capacity of urban surfaces and by the higher land cover homogeneity within the corresponding pixels in comparison to pixels reflecting peri-urban stations. Moreover, the study demonstrated that higher-order regression and neural networks models resulted in consistent improvement in terms of the error values as compared to linear models which are typically used in literature. The use of the derived parametric relationships to datasets of the following year was also considered satisfactory. The general performance of the developed models indicate that satellite data of high temporal resolution are an invaluable tool for the estimation of real time, spatially dense  $T_{air}$  fields, with relatively small error.

Nevertheless, there are some methodology limitations that need to be acknowledged. At first, the estimation of  $T_{air}$  using passive remote sensing may be limited due to the presence of clouds. Even in a region like the Athens agglomeration where excessive cloudiness is rather rare especially during summer months, a considerable amount of data was missing (approximately 20%). This results in gaps in the constructed modeled air temperature series, which may set limits to their exploitation. In addition, due to the large spatial variability of the urban thermal environment, it is of great importance to downscale satellite data of coarse resolution, a process that introduces a further error in the calculations. Despite the above limitations, results were satisfactory even for 1 km x 1 km spatial resolutions, at the precondition that the land cover is to a good extent homogeneous, which was the case for most of the examined stations. However larger errors as found in a number of stations may be attributed to inhomogeneous land cover with the pixel of 1 km x 1 km. One more

**Table 4:** Results of 2<sup>nd</sup> order, LST-8 regression model, (validation set: 16.08.14-31.08.14).

Stations	Ampelokipoi	Athens	Kantza	Markopoulo	Maroussi	Penteli	Peristeri
R <sup>2</sup>	0.86	0.85	0.87	0.88	0.88	0.81	0.82
Adjusted R <sup>2</sup>	0.86	0.85	0.87	0.88	0.88	0.81	0.82
RMSE (°C)	1.17	1.11	1.44	1.31	1.22	1.96	1.14
MAE (°C)	0.91	0.84	1.14	1.03	0.97	1.62	0.87
ME (°C)	0.07	0.12	0.17	0.12	0.13	0.10	0.18
NMAE (%)	3.17	2.93	4.19	3.86	3.52	6.25	3.06
NME (%)	0.24	0.41	0.69	0.44	0.47	0.38	0.63

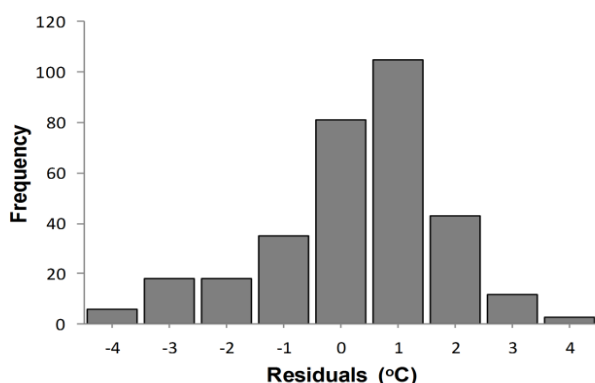


**Figure 7:** Residuals histogram, Ampelokipoi station, 01.07.15 - 31.08.15 (2<sup>nd</sup> order regression, LST-4 predictor set).

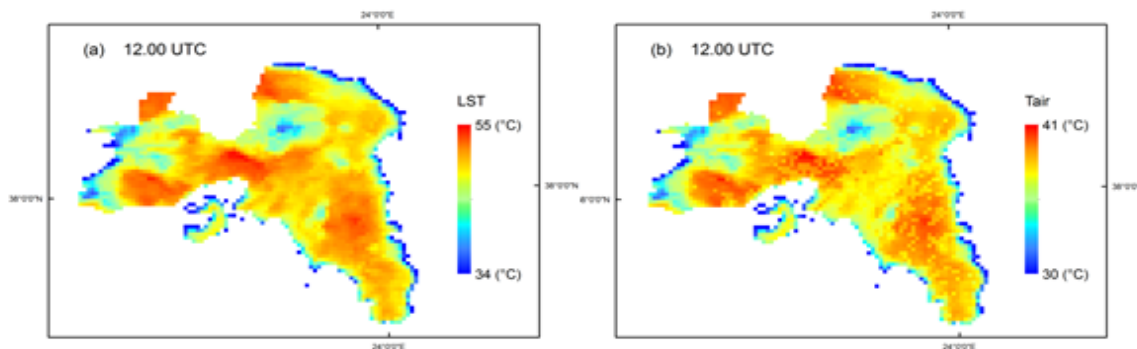


**Figure 8:** Daytime temperature map of Athens agglomeration during heat wave (30.07.2015, 12.00 UTC): a) LST (°C), b) Simulated air temperature (°C).

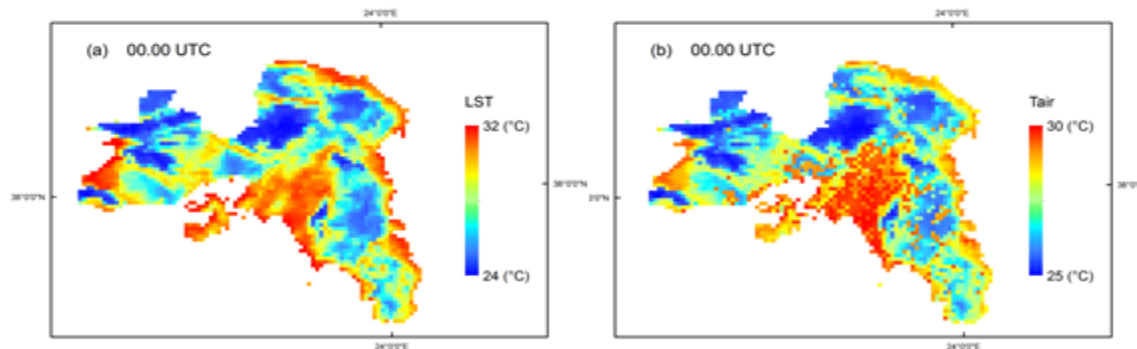


**Figure 9:** Night-time temperature map of Athens agglomeration during heat wave (31.08.2015, 00.00 UTC): a) LST (°C), b) Simulated air temperature (°C).

methodological limitation of the study is that the effect of synoptic scale processes on  $T_{air}$  calculations is not considered. The derived parametric relations describe an average coupling between LST and  $T_{air}$ , but for instance in the case of a strong advection or a frontal passage, a quite different correlation between LST and  $T_{air}$  should be expected. Errors are expected to decrease, if weather conditions area also considered.

The methodology reflects a valuable approach for the estimation of  $T_{air}$  from LST whereas it facilitates a wide variety of applications for the examined urban agglomerations, including the estimation of thermal discomfort, the cooling/heating degree days, the spatial variability of energy needs, etc. It should be mentioned, that the parametric relations as extracted from the above methodology are in principle applicable for a specific station, as they depend on the land cover and the associated land surface characteristics. However the performed analysis has shown that they may be also used for stations in areas with similar land cover and in the same climatic zone. Further research is needed to this direction, taking also into consideration additional parameters (such as urban density, type of surface materials) with the potential to influence the relationship between LST and  $T_{air}$ .

#### Acknowledgements

Part of this study was conducted within the project MONITOR (ESA-MOST Dragon Program). The authors wish to thank Dr. I. Keramitsoglou, Researcher at the National Observatory of Athens, for the provision of the MSG-SEVIRI data."

#### References

1. Voogt JA, Oke TR (2003) Thermal remote sensing of urban climates. *Remote Sens Environ* 86: 370-384.
2. Mihalakakou G, Santamouris M, Papanikolaou N, Cartalis C and Tsangrassoulis A (2004) Simulation of the Urban Heat Island Phenomenon in Mediterranean Climates. *Pure Appl Geophys* 161: 429-445.
3. Santamouris M (2014) Cooling the cities—A review of reflective and green roof mitigation technologies to fight heat island and improve comfort in urban environments. *Solar Energy* 103: 682-703.
4. Keramitsoglou I, Kiranoudis CT, Ceriola G, Weng Q, Rajasekar U (2011) Identification and analysis of urban surface temperature patterns in Greater Athens, Greece, using MODIS imagery. *Remote Sens Environ* 115: 3080-3090.
5. Founda D, Pierros F, Petrakis M, Zerefos C (2015) Interdecadal variations and trends of the Urban Heat Island in Athens (Greece) and its response to heat waves. *Atmos Res* 161-162: 01-13.
6. Rapsomanikis S, Trepekli A, Loupa G, Polyzou C (2015) Vertical Energy and Momentum Fluxes in the Centre of Athens, Greece During a Heatwave Period (Thermopolis 2009 campaign). *Bound-Layer Meteorol* 154: 497-512.
7. Kourtidis K, Georgoulas AK, Rapsomanikis S, Amiridis V, Keramitsoglou I, et al. (2015) A study of the hourly variability of the urban heat island effect in the Greater Athens Area during summer. *Sci Total Environ* 517: 162-177.
8. Giannaros TM, Melas D, Daglis IA, Keramitsoglou I, Kourtidis K (2013) Numerical study of the urban heat island over Athens (Greece) with the WRF model. *Atmos Environ* 73: 103-111.
9. Giannaros TM, Melas D, Daglis IA, Keramitsoglou I (2014) Development of an operational modeling system for urban heat islands: an application to Athens, Greece. *Nat Hazards Earth Syst Sci* 14: 347-358.
10. Kassomenos PA, Katsoulis BD (2006) Mesoscale and macroscale aspects of the morning Urban Heat Island around Athens, Greece. *Meteorog Atmos Phys* 94: 209-218.
11. Santamouris M, Papanikolaou N, Livada I, Koronakis I, Georgakis C, et al. (2001) On the impact of urban climate to the energy consumption of buildings. *Solar Energy* 70: 201-216.
12. Skoulika F, Santamouris M, Kolokotsa D, Boemi N (2014) On the thermal characteristics and the mitigation potential of a medium size urban park in Athens, Greece. *Landsc Urban Plan* 123: 73-86.
13. Santamouris M (2014) On the energy impact of urban heat island and global warming on buildings. *Energy and Buildings* 82: 100-113.
14. Santamouris M (2015) Regulating the damaged thermostat of the cities – status, impacts and mitigation strategies. *Energ Buildings* 91: 43-56.
15. Stathopoulou E, Mihalakakou G, Santamouris M, Bagiorgas HS (2008) On the Impact of temperature on tropospheric ozone concentration levels in urban environments. *J of Earth Sys Science* 117: 227-236.
16. Pantavou K, Theoharatos G, Mavrakis A, Santamouris M (2011) Evaluating thermal comfort conditions and health responses during an extremely hot summer in Athens. *Build Environ* 46: 339-344.
17. Kikon N, Singh P, Singh SK, Vyas A (2016) Assessment of urban heat islands (UHI) of Noida City, India using multi-temporal satellite data. *Sustainable Cities and Society* 22: 19-28.
18. Chen E, Allen Jr. LH, Bartholic JF, Gerber JF (1983) Comparison of winter-nocturnal geostationary satellite infrared-surface temperature with shelter-height temperature in Florida. *Remote Sens Environ* 13: 313-327.
19. Green RM, Hay SI (2002) The potential of Pathfinder AVHRR data for providing surrogate climatic variables across Africa and Europe for epidemiological applications. *Remote Sens Environ* 79: 166-175.
20. Nieto H, Sandholt I, Aguado I, Chuvieco E and Stisen S (2011) Air temperature estimation with MSG-SEVIRI data: Calibration and validation of the TVX algorithm for the Iberian Peninsula. *Remote Sens Environ* 115: 107-116.
21. Wloczyk C, Borg E, Richter R, Miegel K (2011) Estimation of instantaneous air temperature above vegetation and soil surfaces from Landsat 7 ETM+ data in northern Germany. *Int J Remote Sens* 32: 9119-9136.
22. Pichierri M, Bonafoni S, Biondi R (2012) Satellite air temperature estimation for monitoring the canopy layer heat island of Milan. *Remote Sens Environ* 127: 130-138.
23. Bechtel B, Wiesner S, Zaksek K (2014) Estimation of Dense Time Series of Urban Air Temperatures from Multitemporal Geostationary Satellite Data. *J Sel Top Appl Earth Obs Remote Sens* 7: 4129-4137.
24. Good E (2015) Daily minimum and maximum surface air temperatures from geostationary satellite data. *J Geophys Res Atmos* 120: 2306-2324.
25. Sun YJ, Wang JF, Zhang RH, Gillies RR, Xue Y, et al. (2005) Air temperature retrieval from remote sensing data based on thermodynamics. *Theor Appl Climatol* 80: 37-48.
26. Keramitsoglou I, Kiranoudis CT, Weng Q (2013) Downscaling geostationary Land Surface Temperature Imagery for Urban Analysis. *IEEE Geosci Remote Sens Lett* 10: 1253-1257.
27. Keramitsoglou I, Kiranoudis CT, Sismanidis P (2014) Towards real time quarter-hour monitoring of the urban thermal environment at sharpened spatial resolution. *Proc 3<sup>rd</sup> Int. Workshop EORSA* 105-110.
28. European Environmental Agency (2010) Data and Maps/Datasets/Urban Atlas.

#### Author Affiliation

Top

<sup>1</sup>Department of Environmental Physics and Meteorology, National and Kapodistrian University of Athens, Greece